2014-01-01

Integrating Two-Photon Microscopy And Cryo-Electron Microscopy For Studying The Interaction Of Caféteria Roenbergensis And CroV

Seyedmohammadali Aghvami
University of Texas at El Paso, aliaghvami81@yahoo.com

INTEGRATING TWO-PHOTON MICROSCOPY AND CRYO-ELECTRON MICROSCOPY FOR STUDYING THE INTERACTION OF CAFÉTERIA ROENBERGENSIS AND CROV

SEYEDMOHAMMADALI AGHVAMI

Department of Physics

APPROVED:

Chunqiang Li, Ph.D., Chair

Chuan Xiao, Ph.D.

Marian Manciu, Ph.D.

Charles H. Ambler, Ph.D.
Dean of the Graduate School

INTEGRATING TWO-PHOTON MICROSCOPY AND CRYO-ELECTRON MICROSCOPY FOR STUDYING THE INTERACTION OF CAFÉTERIA ROENBERGENSIS AND CROV

by

SEYEDMOHAMMADALI AGHVAMI,

THESIS

Presented to the Faculty of the Graduate School of

The University of Texas at El Paso

in Partial Fulfillment

of the Requirements

for the Degree of

MASTER OF SCIENCE

Department of Physics

THE UNIVERSITY OF TEXAS AT EL PASO

August 2014

Acknowledgements

First and foremost I offer my sincerest gratitude to my supervisor, Dr. Chunqiang Li, who has supported me throughout my thesis with his patience and knowledge. Moreover, I thank Dr. Chuan Xiao not only for providing us with the samples, but also because of offering much advice during our weekly meetings. Gratitude goes to Dr. Marian Manciu for his support and being part of the thesis committee. I also thank Dr. Eric Hagedorn, Dr. Vivian Incera, and Dr. Efrain Ferrer for their help and advices during my study at UTEP. Finally I thank my wife and my family for always offering help and support.

Table of Contents

List of Tables

List of Figures

Chapter 1: Introduction

Viral abundance in the ocean ranges from approximate 10^7 to 10^{10} L^{-1}, and 10^7 to 10^{10} g^{-1} of dry weight in marine sediments [1, 2]. Being the major cause of mortality in marine microorganisms, marine viruses have been shown to play critical roles, directly and indirectly, in natural microbial communities in the oceans [2, 3]. Therefore, marine viruses influence nutrient recycles, impact genetic diversity in oceans [2, 4] and might also affect the climate changes [1].

Viral infections are extremely abundant in oceans, estimated to be 10^{23} per second [3]. Viral infection in marine are largely unknown, and very little research has been done on viewing the infection process between marine viruses and their hosts. It is still a mystery for the first step of the infection about how the viruses get into the host, whether it is going through the phagocytosis or penetrating the host cell membrane directly. In this study we try to get a better resolution of the viral infection of Cafeteria roenbergensis (C. roenbergensis) by Cafeteria roenbergensis virus (CroV) by integrating two imaging modalities; two-photon excitation fluorescence microscopy and cryo-electron microscopy.

CroV and its host, Cafeteria roenbergensis are introduced in this chapter. Theory and setup of imaging modalities are explained in chapters 2 and 3. Chapter 4 explains our methods, images we got and the results.

1.2 Cafeteria Roenbergensis

Cafeteria roenbergensis was discovered by Danish marine ecologist Tom Fenchel and taxonomist David Patterson in 1988. It is found primarily in coastal waters where there are high concentrations of bacteria on which it grazes. Its voracious appetite plays a significant role in regulating bacteria populations [5]. Tom Fenchel, is credited with having joked about the chromalveolate's name: "We found a new species of ciliate during a marine field course in Rønbjerg and named it Cafeteria roenbergensis because of its voracious and indiscriminate appetite after many dinner discussions in the local cafeteria." —Tom Fenchel [6].

Cafeteria roenbergensis is a small bacterivorous marine flagellate. Bacterivores are free-living organisms, exclusively microscopic, which obtain energy and nutrients primarily or entirely from the consumption of bacteria. Similar to other flagellates it has whip-like organelles called flagella which are used for gathering food.

Cafeteria roenbergensis is a slightly flattened, kidney-shaped bicosoecid (small group of unicellular flagellates). Its cell typically measures between 3 and 10 μm and it has a volume of around 20 μm^3 [7]. It is colorless and has two unequally sized flagella. Cafeteria is a eukaryotic organism, so it contains the typical organelles such as mitochondria and nuclei [7].

Cafeteria roenbergensis is a suspension feeder, meaning it feeds by filtering suspended bacteria, its primary food source, and other particulate matter from the water [8]. Its two flagella facilitate feeding, locomotion and attachment to substrates. The anterior flagellum is responsible for locomotion and feeding. It propels the cell in a swift spiral movement. During feeding, it beats at about 40 times per second to create a current of water that moves about 100 micrometers/second. This current brings bacteria to its mouthparts. The food is ingested below the base of the flagella, which is referred to as the ventral side [9].

Bacterivorous nanoflagellates, the general group to which C. roenbergensis belongs, make up a significant portion of the oceans' protozoan communities, as well as those in freshwater, soils and other habitats. They are reported to be the primary consumer of bacteria in many habitats, controlling bacterial populations as they "graze"[10].

Because they are easy to grow in culture, Cafeteria roenbergensis has been subject to a diversity of more detailed studies, such as genomic and ecological studies that have revealed that this species has the most functionally compact DNA amongst eukaryotes [5]. While in culture, Cafeteria are fed Vibrio bacteria. In a test conducted by Park and Simpson in 2010, it was found that Cafeteria cells grow best in salinities of 3 ppm to 100 ppm, but cannot survive at concentrations any higher [11].

1.3 CAFETERIA ROENBERGENSIS VIRUS

Cafeteria roenbergensis virus (CroV) is the giant virus that infects the marine zooplankton Cafeteria roenbergensis [12]. CroV has one of the largest genome of all marine virus known, consisting of ~730,000 base pairs of double-stranded DNA. Among its 544 predicted protein-coding genes are several that are usually restricted to cellular organisms, such as translation factors and enzymes for DNA repair and carbohydrate synthesis. CroV is distantly related to Mimivirus and belongs to a group of viruses known as Nucleocytoplasmic large DNA viruses [13].

CroV is a giant virus and has an important effect on the mortality of Cafeteria roenbergensis populations. The study done at 2010 found that this virus only attacked Cafeteria cells, leaving many similar organisms unharmed [14].

1.4 INTERACTION BETWEEN C. ROENBERGENSIS AND CROV

Since CroV attacks C.roenbergensis only, and leave many other similar organisms unaffected [15], this specific infection between C.roenbergensis and CroV would be a perfect host-virus interaction system to explore viral infection. However, C.roenbergensis swims fast, in addition, the infection speed between C.roenbergensis and CroV are also very fast and complicated, therefore, there are many difficulties and challenges for traditional imaging techniques to view viral-host interaction.

Optical multiphoton microscopy (MPM) is opening new windows for biomedical research [16]. Two-photon fluorescence microscopy (TPFM) is one example of such novel optical imaging technology. TPFM is a very attractive tool for scientists to explore dynamic processes in vivo at a cellular level [17].

The benefits by using TPFM are from the ability of optical sectioning, deeper tissue penetration and less photobleaching and photodamage [18]. The lateral resolution of TPFM could be as high as several hundred nanometers [19]; by using fast scanning approaches, the

imaging speed of the TPFM could reach to real-time video rate [20]. Therefore, it is a suitable optical live imaging modality to monitor the interaction between fast moving viruses and hosts.

Cryo-electron microscopy on the other hand, is shown to be a high resolution imaging modality that can preserve the specimen in a state closer to its native state. The viral particles can be imaged free from damage of dehydration or adsorption to a support that is encountered in preparing biological samples method [21]. Integrating these two imaging modalities provides us with a strong tool for studying this interaction, where it benefits from real-time video rate imaging capability of TPFM and nanometer resolution of electron microscopy.

Chapter 2: Two-Photon Excitation Fluorescence Microscopy

The theoretical concept of multiphoton excitation was first proposed by physicist Maria Göppert-Mayer in 1931 [22] but was not experimentally proven until the invention of the laser 30 years later, and even then, it required decades of further development in laser technology to become of practical utility. The fields of physical chemistry and physics were the first to apply this technique [23], and biological research has only more recently embraced multiphoton excitation to image living cells [24]. Biological uses of multiphoton microscopy have been extensively reviewed [25].

2.1 Fluorescent Microscopy

Fluorescent microscopy is very popular for imaging biological samples because of specific characteristics of fluorescent molecules. Samples reveal fluorescent through exogenous labeling or endogenous autofluorescence. Spatial and functional information can be obtained through absorption, emission, lifetime and other contrasts in fluorescence microscopy. As shown in figure 2.1, the fluorescent molecule is excited to the higher electronic state by absorbing a photon where after a short time it decays to lower state by emitting fluorescent light. In a single photon event, the energy of the excitation light should be equal to the molecule energy gap ΔE_g, and considering the relationship between photon energy and E and radiation wavelength λ, it follows that

$$\Delta E_g = E = \frac{hc}{\lambda} \qquad (2.1)$$

where $h = 6.6 \times 10^{-34}\ J.s$ is Planck's constant and $c = 3 \times 10^{8}\ m/s$ is the speed of light in the vacuum.

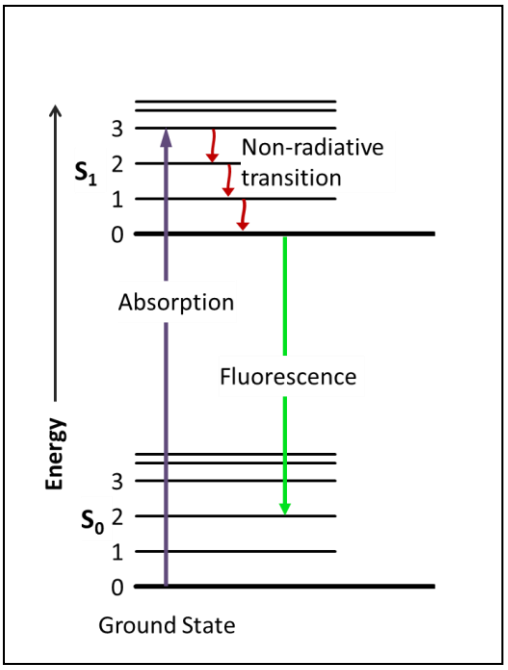

Figure 2.1 Energy levels of a fluorescent molecule

In conventional fluorescence microscopes, sample is illuminated by ultraviolet or visible light and excitation happens when energy of the absorbed photon matches with the energy gap from the ground state to the excited state. The illumination light is separated from the much weaker emitted fluorescence through the use of a dichroic mirror.

August Köhler constructed the first ultraviolet (UV) microscope at Zeiss optical Works in Jena Germany, in 1904. Inspired by Abbe's finding that shorter wavelength light results in better resolution, he used UV to illuminate the sample, where he also noted that some objects emitted light of a longer wavelength than illumination light. However, it was the physicist Oskar Heimstädt who, in 1911, used this observation as the basis for the construction of the first successful fluorescence microscope [26].

Fluorescence imaging is widely used for morphological and functional studies in biology. However; since in-focus structures are washed out by fluorescence outside the plane of focus, images obtained by conventional (single-photon) fluorescence microscopy do not have the expected quality. Although using a thin sample will result in better image, this approach is clearly inapplicable for living tissue. The introduction of confocal microscopy has been an important advance, providing an "optical-sectioning" effect by using a pinhole aperture to reject

out-of-focus fluorescence [27]. But imaging depth of confocal microscopy is limited and due to the use of short (high-energy) excitation wavelengths, photodamage and photobleaching are still there. Development of multiphoton excitation greatly minimized these problems while it is capable of the optical-sectioning same as confocal microscopy [28].

2.2 Pulsed Laser for Two-photon Excitation

Figure 2.2 shows the energy diagram of two-photon excitation of a fluorescent molecule (right) and its comparison to one-photon excitation (left).

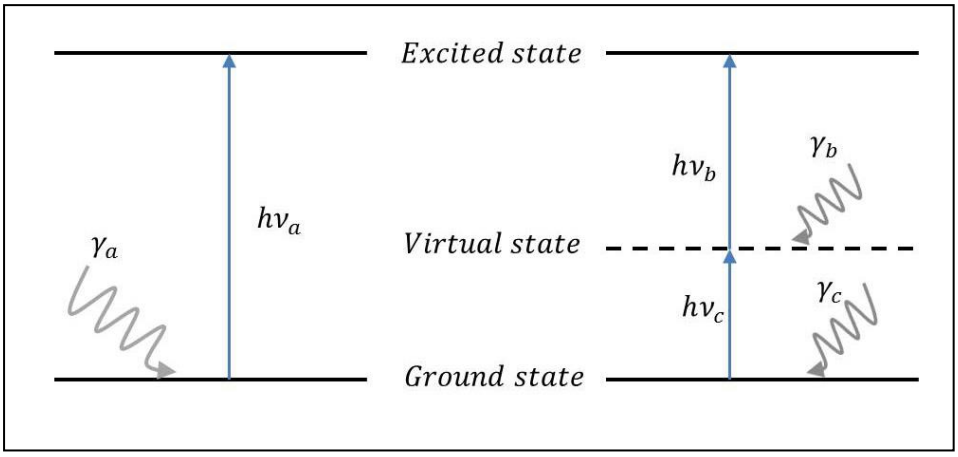

Figure 2.2 One-photon and two-photon excitation

In two-photon excitation process fluorescence molecule is excited to the higher electronic level by simultaneously receiving two low energy photons. These two photons are not necessarily identical, but their wavelengths, λ_1 and λ_2, have to be such that

$$\lambda_{1P} \cong \left(\frac{1}{\lambda_1} + \frac{1}{\lambda_2}\right)^{-1} \qquad (2.2)$$

where λ_{1P} is the wavelength of the single photon excitation process of the same molecule. However, for much easier practical implementation they can be chosen to have the same wavelength given by

$$\lambda_1 = \lambda_2 \approx 2\lambda_{1P} \qquad (2.3)$$

and

$$\Delta E_g = \frac{2hc}{\lambda_{1P}} \qquad (2.4)$$

Assuming a virtual intermediate state, the resident time in the intermediate state, τ_{virt}, can be found by using time-energy uncertainty consideration for two-photon excitation:

$$\Delta E_g . \tau_{virt} \cong \hbar/2 \qquad (2.5)$$

where $\hbar = h/2\pi$. The temporal window available to two photons to coincide in the virtual state is then:

$$\tau_{virt} \cong 10^{-15} - 10^{-16} s \qquad (2.6)$$

This means that in a two-photon excitation process, it is crucial to combine sharp spatial focusing with temporal confinement in the virtual state [29]. With higher photon densities which are temporally and spatially confined, the process can be extended to n-photon excitation. Hence, fluorescent molecules with UV and visible one photon excitation transitions can be excited by near-infrared (680-1100) nm photons. Typical photon flux densities can be found to be of the order of 10^{24} photons/cm^2s, which implies intensities around $MW - TW / cm^2$ [22].

A theoretical model of two-photon excitation has been proposed by Nakamura [30] using perturbation for a time-dependent Schrodinger equation, where Hamiltonian contains electric dipole interaction terms. The first-order solution is found to be related to one-photon excitation, and higher order solutions are related to n-photon excitation ones from which the dependence of two-photon excitation fluorescence on I^2 is obvious[31].

Considering δ_2 as the molecular cross-section, the relation between fluorescence intensity per molecule, $I_f(t)$, and the intensity of the excitation beam, $I(t)$, then can be shown as:

$$I_f(t) \propto \delta_2 . I(t)^2 \propto \delta_2 . P(t)^2 \left[\pi \frac{(NA)^2}{hc\lambda}\right]^2 \qquad (2.6)$$

where $P(t)$ is the laser power and (NA) is the numerical aperture of the focusing objective lens and distribution of photons in time and space is treated in the last term by using the paraxial approximation in an ideal optical system [32].

For a continuous wave (CW) laser excitation, the time-averaged two-photon fluorescence intensity per molecule within an arbitrary time interval T, $< I_f(t) >$ can be written as:

$$< I_f(t) > = \frac{1}{T}\int_0^T I_f(t)\, dt \propto \delta_2 . \left[\pi \frac{(NA)^2}{hc\lambda}\right]^2 \frac{1}{T}\int_0^T P(t)^2\, dt \qquad (2.7)$$

Considering $P_{avg} = P(t)$, equation (1.7) can be transformed into

$$< I_{f,CW}(t) > \propto \delta_2 . P_{avg}^2 \left[\pi \frac{(NA)^2}{hc\lambda} \right]^2 \quad (2.8)$$

For the ultrafast pulsed laser time duration T in equation (2.7) can be considered as $1/f_P$, where f_P is the pulse repetition rate. Considering $D = \tau_P . f_P$, where τ_P pulse width of the pulsed laser beam, average power is

$$P_{avg} = D. P_{peak}(t) \quad (2.9)$$

and the approximated $P(t)$ profile can be described as

$$P(t) = \frac{P_{avg}}{D} \qquad \text{for } 0 < t < \tau_P$$

$$P(t) = 0 \qquad \text{for } \tau_P < t < (1/f_P) \quad (2.10)$$

Thus, we can write eq. (2.7) as

$$< I_{f,P}(t) > \propto \delta_2 . \frac{P_{avg}^2}{\tau_P^2 f_P^2} \left[\pi \frac{(NA)^2}{hc\lambda} \right]^2 \frac{1}{T} \int_0^{\tau_P} dt = \delta_2 . \frac{P_{avg}^2}{\tau_P^2 f_P^2} \left[\pi \frac{(NA)^2}{hc\lambda} \right]^2 \quad (2.11)$$

Comparing eq. (2.8) and (2.11) shows that for the same efficiency of CW and pulsed lasers, the average power of CW must be kept higher by a factor of $1/\sqrt{\tau_P . f_P}$. This means that 10W of CW laser will be nearly equivalent to 30 mW of the pulsed lase to allow the same efficiency of approximately 10^{-1} mW [33].

2.3 Advantages of Two Photon Fluorescence Microscopy

2.3.1 3D Sectioning

The 3D confinement of the two-photon fluorescence (TPF) volume can be understood through optical diffraction theory. The intensity distribution of the excitation beam with wavelength λ at the focal region of an objective is described

$$I(u, v) = \left| 2 \int_0^1 J_0(vp) e^{-(i/2)u\rho^2} \rho d\rho \right|^2$$

Where J_0 is the zeroth-order Bessel function, ρ is a radial coordinate in the pupil plane, and $u = 8\pi\sin^2\left(\frac{\alpha}{2}\right)z/\lambda$ and $v = 2\pi\sin(\alpha)r/\lambda$ are dimensionless axial and radial coordinates, respectively normalized to the wavelength.

The intensity of fluorescence distribution within the focal region is proportional to $I(u, v)$ for the one-photon and $I^2(u/2, v/2)$ for the TPF. Integrating over v, keeping u constant will have a half-bell shaped result for TPF where for one-photon case the behavior is constant along z axis. This confinement of the TPF distribution intensity was shown for the first time in 1990 by Sheppard and Gu [34].

The most interesting aspect of is that the excitation power falls off as the square of distance from the lens focal point [35]. Considering the quadratic relation between the excitation power and the fluorescent intensity, TPF will fall off as the forth power of distance from the focal point of the objective lens. Hence, TPF microscopy is intrinsically three dimensional and its optical sectioning effect is obtained in a very different way with respect to confocal solution.

2.3.2 Advantages of Using a Longer Wavelength

Confinement of the fluorescent emission in TPF microscopy also confines photobleaching to the plane of focus. However, several major advantages occur secondarily from the use of long excitation wavelengths.

Deeper Penetration

Light scattering declines steeply with increasing wavelength, so that infrared light (700–1,000 nm) used for two-photon imaging penetrates much deeper into tissue (~500 μm) than the equivalent blue light (350–500 nm) used for one-photon excitation [24,27].

Less Photodamage to the Sample

Infrared light causes negligible photodamage or phototoxicity to cells. This is particularly advantageous for fluorophores and endogenous proteins that would normally require excitation at short (<300 nm) and highly damaging ultraviolet wavelengths but can be made to fluoresce by three-photon excitation at infrared wavelengths three times longer [36].

Simultaneous Imaging of Two or More Fluorophores

The two-photon excitation spectra of most fluorophores are broader than for one-photon excitation, so a single multiphoton excitation wavelength can be used to simultaneously excite multiple fluorophores with distinct emission wavelengths [25].

2.4 SCANNING LASER TWO-PHOTON EXCITATION FLUORESCENCE MICROSCOPE SETUP

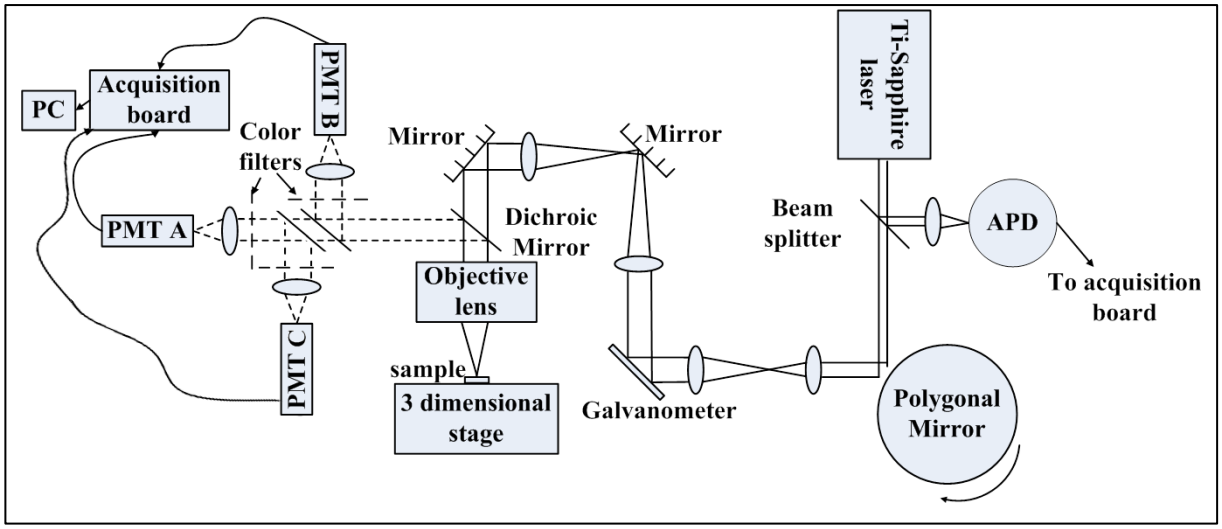

Figure 2.3 Schematic of laser scanning two-photon microscope at UTEP Biophotonics lab

Schematic of our TPFM setup is shown in figure 2.3. Major parts of this setup are briefly explained in this section

2.4.1 Laser Source

Figure 2.4 shows the Ti:sapphire laser source (Newport, Spectra-Physics Maitai HP) of our setup. The emission range between 700 nm and 1020 nm of the Ti:sapphire laser allows a large number of commonly used fluorescent molecules to be excited. Similar to other laser sources used for TPF microscopy, it works in the mode-locking mode. The basis of this technique is to induce a fixed phase relationship between the longitudinal modes of the

laser's resonant cavity. Interference between these modes causes the laser light to be produced as a pulse train of 80 MHz, with each pulse having a pulse width of about 100 fs.

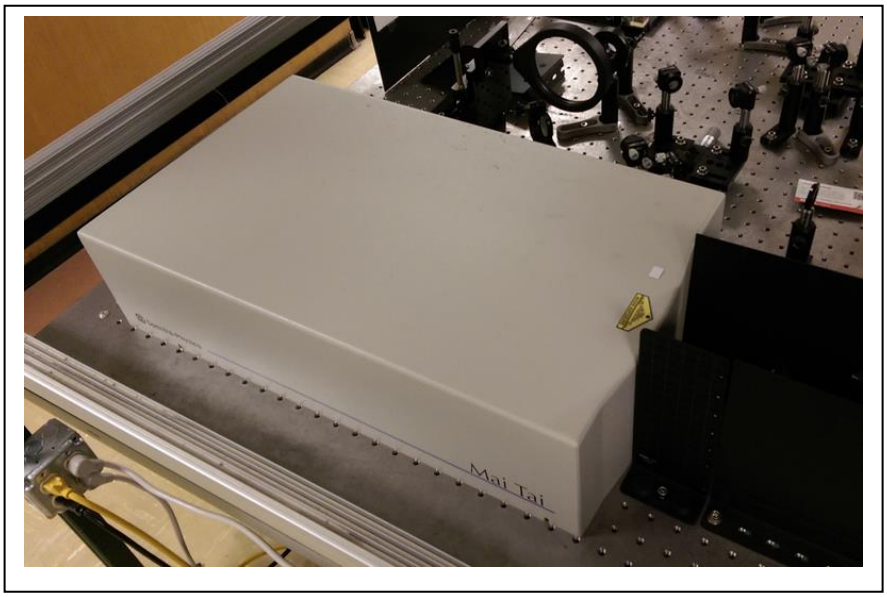

Figure 2.4 Ti:sapphire laser

Figure 2.5 shows the laser emission time scale for two-photon excitation. A short pulse at high photon density is released for approximately 100 fs. This laser shot is able to prime fluorescence without damaging the sample so fluorescence occurs in the next few nanoseconds. The laser is silent for 10 ns and then delivers a new high-density photon pulse. This modality allows TPF to be experienced at tolerable time-averaged power.

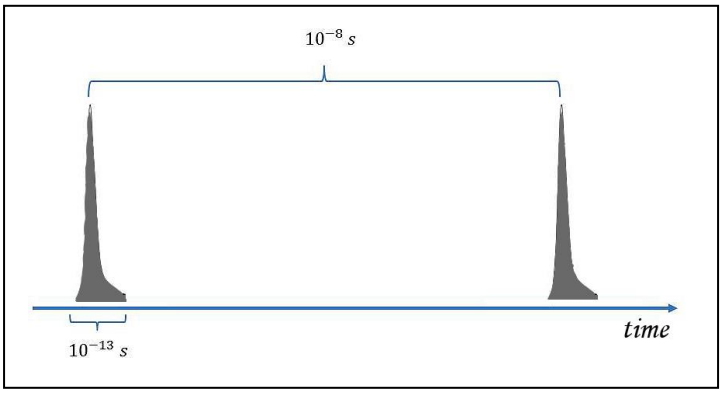

Figure 2.5 Laser emission time scale

2.4.2 Video Rate Imaging with Scanning TPF Microscope

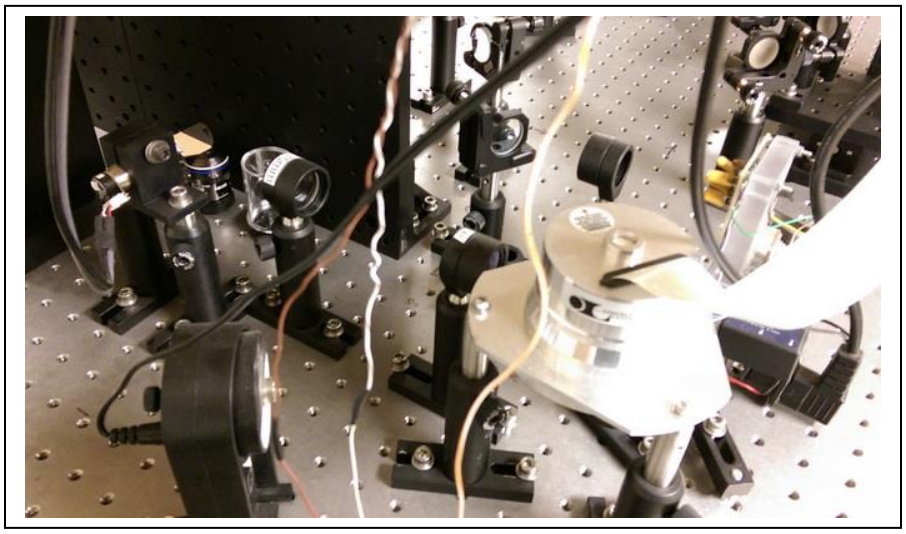

Figure 2.6 Raster scanning setup

In order to image fast biological interactions, image requisite rate of our microscope is set to be 30 frames per second and it can be increased to 120 frames per second. In our scanning microscope, images are built by raster scanning the x-y plane by the fast rotating polygon mirror synchronized with a galvanometer mirror. This combination has brought the 30 frames per second video imaging capability to our system. 480 revolutions per second of 36 facet polygon mirror, scans x axis, making 17280 lines. These lines are arranged in y axis by the 30 Hz galvanometer mirror allowing 30 frames per second images where each image consist of 576 lines. This combination is shown Figure 2.6.

2.4.3 Three Channels of Fluorescence Imaging Using Different PMTs

Photomultiplier tube (PMT) is an extremely sensitive detector of light, suitable for scanning fluorescent microscopy. These detectors multiply the current produced by incident light by as much as 100 million times, in multiple dynode stages, enabling individual photons to be detected when the incident flux of light is very low. This point-like intensity is then interpreted and produces a corresponding point of light on the monitor.

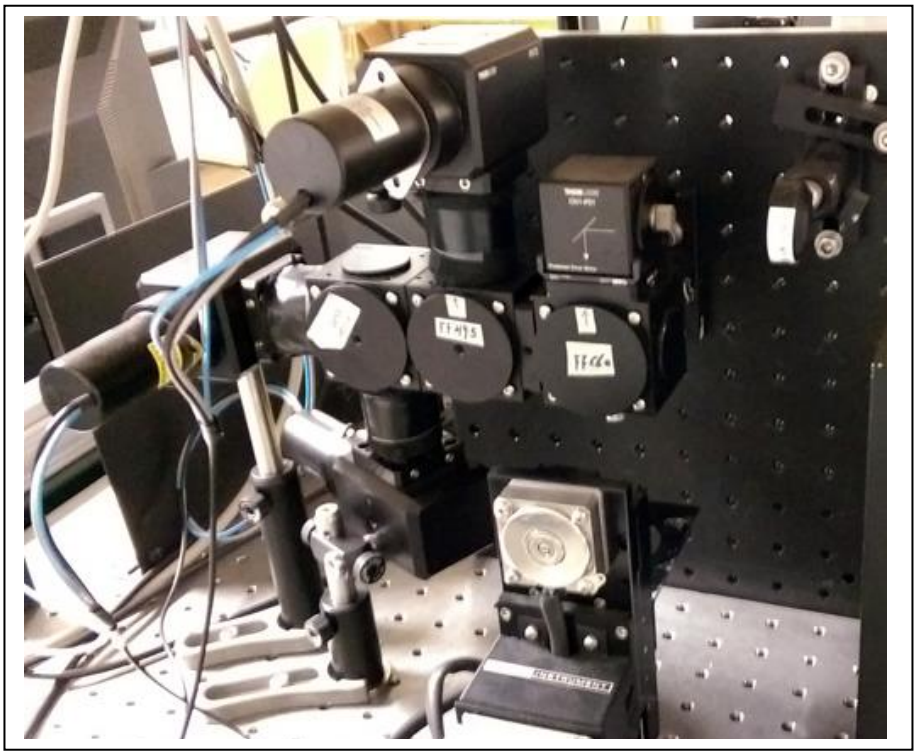

Figure 2.7 Three channels of TPF microscope

To study the interaction between different biological object, we need to distinguish their fluorescence emission. These objects are required to be imaged simultaneously which needs a setup capable of imaging different fluorescent wavelengths at the same time. Different fluorescent wavelengths are separated by mean of dichroic mirrors and are then transmitted through a filter. Each beam of light is then detected by a photomultiplier tube (PMT). The voltage of these three PMTs is controlled by three customized power suppliers, correspondingly. Different fluorescence signals are acquired simultaneously by a frame grabber (Matrox Solios eA/XA) and recorded on personal computer at 30 frames/s. Figure 2.7 shows these three PMTs; blue, green and red channels that allow us to image different fluorescent signals simultaneously.

A reflection channel is also built by placing a beam splitter before the polygonal mirror and an avalanche photo-diode (HAMAMATSU,S2381) is used to collect the reflection signal from the sample. The reflection signal is acquired by the frame grabber and recorded on computer.

Chapter 3: Cryo-Electron Microscopy

3.1 The History of Electron Microscopy

In 1926 Busch showed theoretically that a short solenoid is able to converge a beam of electrons. It opened a new era in microscopy where, using electrons instead of light could bring a better resolution. It was accepted that it was simply not possible to resolve structures of less than half a micrometer with a light microscope because of the Abbe's formula. The first electron image was taken by German engineers Ernst Ruska and Maximillion Knoll in 1931. Two years later in 1933, Ruska built the first electron microscope which was capable of resolving about 50 nm.

Because a very high current density of the electron beam was concentrated into a very small area, the early electron microscopes were not suitable for imaging biological samples and charred any non-metallic specimens that were examined. However, the electron microscope began to appear as a viable proposition after it became successful in examining the biological specimens by treating them with osmium and cutting very thin slices of the sample. Development of electron microscopy led to arise of commercial electron microscopes which were capable of 1 nm resolution in the middle of twentieth century [37].

3.2 Types of Electron Microscopes

3.2.1 Transmission Electron Microscope

Transmission Electron Microscopy (TEM) uses a thin sample illuminated by a highly collimated kilovolt electron beam. The high voltage electron beam which is emitted by a cathode and formed by magnetic lenses is then partially transmitted through the very thin semitransparent (for electrons) specimen. This beam carries information about the structure of the specimen. The high-resolution image which is the spatial variation in this information is then magnified by a series of magnetic lenses and finally recorded by hitting a fluorescent screen, photographic plate, or light sensitive sensor such as a CCD camera. The CCD image could be displayed in real time on a monitor or computer.

3.2.2 Scanning Electron Microscope

A scanning electron microscope (SEM) produces images of a sample by scanning it with a focused beam of electrons. The electrons interact with atoms in the sample, producing various signals that can be detected and that contain information about the sample's surface topography and composition.

In Scanning Electron Microscope, electrons are not transmitted through the sample like TEM, but the image is produced by detecting secondary electrons which are emitted from the surface due to excitation by the primary electron beam. In the SEM, the electron beam is raster scanned across the surface of the sample and the image is constructed by mapping the detected signals with beam position. SEM usually uses much lower accelerating voltages (1-5kV) for imaging biological samples. Since the secondary electrons are generated from the true surface structure of a sample, this lower voltage is necessary in order to prevent beam penetration into the sample.

3.3 IMAGE FORMATION IN TEM

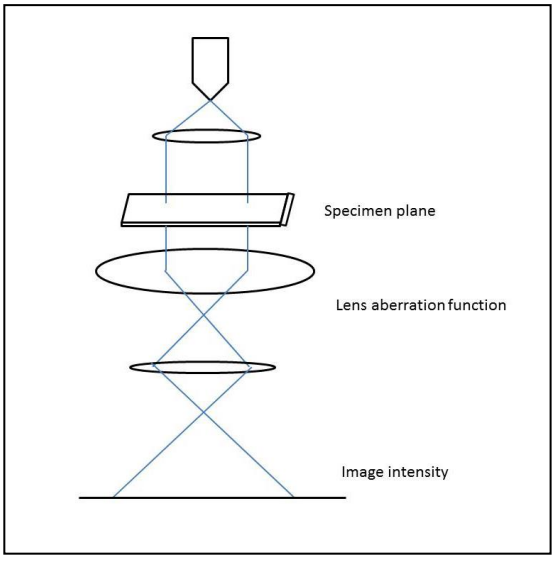

Figure 3.1 Schematic of formation of a TEM image

Figure 3.1 shows a schematic of the overall process in the formation of a TEM image. After the electron scattering in the specimen, image is formed on the image plane. A diffraction

pattern in also formed in the back focal plane of the objective lens which is mathematically related to the image by Fourier transform operations.

Complex mathematics and computational treatment is needed to describe each step in general case. Considering a simple case of imaging a thin specimen and neglecting absorption, the only change to the incident electron beam will be the alteration in its phase not in its amplitude. This phase object approximation (POA) ignores the Fresnel diffraction within the specimen but includes the effect of multiple scattering. Hence the specimen exit-wave complex amplitude can be written as

$$\Psi_e(x,y) = \exp\{-i\sigma\Phi_P(x,y)\} \qquad (3.1)$$

where σ is an interaction constant given by

$$\sigma = 2\pi me\lambda_r/h^2 \qquad (3.2)$$

in which both m and λ_r are relativistically corrected values of the electron mass and wavelength and $\Phi_P = \int_{-1/2}^{1/2} \Phi(x,y,z)dz$ is the two dimensional projection of the specimen potential along the beam direction.

As shown in eq. (3.1) the effect of the specimen is considered to be advancing the phase of the electron wave by $\sigma\Phi_P(x,y)$ over the wave in vacuum. Considering a thin specimen of low atomic number, the values of the mean inner potential are so small that this phase advance is so small and can be expanded as

$$\Psi_e(x,y) = 1 - i\sigma\Phi_P(x,y) \qquad (3.3)$$

This is called weak phase object approximation (WPOA), which assumes kinematic scattering within the specimen requiring that the intensity of the central unscattered beam is significantly stronger than that of the diffracted beam.

The complex amplitude of the scattered wave in the back focal plane of the objective lens can be found by the Fourier transform of Eq. (3.3). With $\Phi_P(x,y)$ real this gives

$$\Psi_d(u,v) = \delta(u,v) - i\sigma\mathcal{F}\{\Phi_P(x,y)\} \qquad (3.4)$$

Considering the presence of the limiting objective aperture P(u,v), and phase shift introduced by the lens which is parameterized by the coefficient of a wave aberration function, $W(u, v)$, the complex amplitude under WPOA is given by

$$\Psi'_d(u, v) = \delta(u, v) - i\sigma\mathcal{F}\{\Phi_P(x, y)\}P(u, v)\exp[iW(u, v)] \quad (3.5)$$

where the presence of a limiting objective aperture is included through the simple function

$$P(u, v) = 1\ \sqrt{u^2 + v^2} \leq r$$
$$P(u, v) = 0\ \sqrt{u^2 + v^2} > r \quad (3.6)$$

Finally the image amplitude (in the image plane) is found by further Fourier transform of Eq. (2.5)

$$\Psi_i(x, y) = 1 - i\sigma\{\Phi_P(-x, y)\}F\{P(u, v)\exp[iW(u, v)]\} \quad (3.7)$$

Since both the sine and cosine of $W(u, v)$ are even, their Fourier transforms are real and hence the recorded image intensity, to the first order, is

$$I(x, y) = \Psi_i(x, y)\Psi_i^*(x, y)$$
$$\approx 1 + 2\sigma\{\Phi_P(-x, -y)\}.\, F\{\sin W(u, v)\, P(u, v)\} \quad (3.8)$$

The above expression shows that for the simplest theory, the image contrast is proportional to the projection of the specimen potential convolved with an impulse response function arising from the instrument [38].

3.4 Resolution of the Electron Microscope

Unlike their optical equivalents there is no simple measure of resolution for the electron microscope, as the resolution depends on both the instrumentation and also on the scattering properties of the sample.

Two-dimensional, black and white images are produced in transmission electron microscopes (TEM). Resolution of the TEM is also limited by spherical and chromatic aberration, but a new generation of aberration correctors has been able to overcome or limit these aberrations. Software correction of spherical aberration has allowed the production of images with sufficient resolution to show carbon atoms in diamond separated by only 0.089 nm and

atoms in silicon at 0.078 nm at magnifications of 50 million times. The ability to determine the positions of atoms within materials has made the TEM an indispensable tool for nano-technologies research and development in many fields, including heterogeneous catalysis and the development of semiconductor devices for electronics and photonics. In the life sciences, it is still mainly the specimen preparation which limits the resolution of what we can see in the electron microscope, rather than the microscope itself.

3.5 SAMPLE PREPARATION

Since the molecules of air would scatter the electrons in an electron microscope, the samples have to be viewed in a vacuum. This means that the samples need to be specially prepared to withstand the environment inside an electron microscope. There are different methods of preparing the sample for electron microscopy where most of them damage the biological specimen. Damage can happen because of dehydration or adsorption onto the supporting film for particles in suspension. Sample preparation technique such as chemical fixation, and negative staining have shown less damaging problems. However these excellent techniques, which are described briefly in this section, change the specimen in order to make it more suitable for electron microscopy. Cryo-fixation, which seems to be the most suitable technique for sample preparation, especially for TEM, is described at last.

3.5.1 Chemical Fixation

Fixation is a general term used to describe the process of preserving a sample at a moment in time and to prevent further deterioration so that it appears as close as possible to what it would be like in the living state, although it is now dead.

In chemical fixation for electron microscopy, glutaraldehyde is often used to crosslink protein molecules and osmium tetroxide is used to preserve lipids. Osmium tetroxide is often used as a secondary fixative when samples are prepared for electron microscopy.

Formaldehyde is a common fixative for light microscopy and is often used on its own. However, for electron microscopy it often doesn't provide enough stability for all of the sample

preparation steps and ultrastructure can be poor. For electron microscopy it is routinely used in combination with glutaraldehyde.

The combination of formaldehyde and glutaraldehyde was presented by a scientist called Karnovsky and has become so popular. "Karnovsky's fixative" is often used in a modified form with lower aldehyde concentrations than originally proposed [39].

3.5.2 Staining and Negative Staining

Since many biological materials are nearly transparent to the electron beam, heavy metals such as lead and uranium are used to scatter imaging electrons and thus give contrast between different structures. By staining the samples with heavy metals, the electron density is increased which results in there being more interactions between the electrons in the primary beam and those of the sample, which in turn make contrast in the resultant image.

In Negative staining, the background is stained, leaving the actual specimen untouched, and thus visible. This contrasts with 'positive staining', in which the actual specimen is stained. The structures which can be negatively stained are much smaller than those studied with the light microscope. Here, the method is used to view viruses, bacteria, bacterial flagella, biological membrane structures and proteins or protein aggregates, which all have a low electron-scattering power. Some stains, such as osmium tetroxide and osmium ferricyanide, are very chemically active. As strong oxidants, they cross-links lipids mainly by reacting with unsaturated carbon-carbon bonds, and thereby fix biological membranes in place in tissue samples while simultaneously stain them [40].

3.5.2 Cryo-fixation

Cryo-electron microscopy where the sample is studied at cryogenic temperatures has been shown as a suitable method for preserving the biological specimen in a state closer to its native state. To overcome all the problems of sample preparation, a simple method is used for preparing and observing frozen-hydrated specimen from native biological suspension [39].

In Cryo-fixation a specimen is rapidly frozen, typically to liquid nitrogen temperatures or below, so the water forms ice without the significant change in the volume. This preserves the specimen in a snapshot of its solution state with the minimal of artifacts. An entire field called Cryo-electron microscopy has branched from this technique. With the development of Cryo-electron microscopy, it is now possible to observe virtually any biological specimen close to its native state.

Chapter 4: Imaging C. Roenbergensis and CroV Interaction

4.1 Preparing C. Roenbergensis and CroV Samples for TPFM

Cafeteria roenbergensis and CroV samples were prepared and cultured at Department of Biomolecular Mechanisms, Max Planck Institute for Medical Research (Heidelberg, Germany) and at UTEP Dr. Xiao's Biochemisty lab by using published protocol [41].

We image Cafeteria roenbergensisin culture by two-photon excited NADH autofluorescence, and we stain CroV with SYBR Gold dye, and image it simultaneously with two-photon by excited SYBR gold fluorescence. Both NADH and SYBR Gold can be excited by using the same laser wavelength at 710nm.

4.1.1 Staining CroV Sample

Among the nucleic acid stains which are used in studying viruses, DAPI (4',6-diamidino-2-phenylindole) has evolved as a useful stain for enumeration of virus particles by fluorescence microscopy [42]. Nucleic acid stains SYBR Green and SYBR Gold are also used for determination of viral and bacterial abundance [41,43], but a comparison between SYBR I Green and SYBR Gold stains has shown a greater persistence of fluorescence signal with SYBR Gold [43].

SYBR Gold stain is superior sensitive for staining DNA and RNA due to the high fluorescence quantum yield of the dye-nucleic acid complexes (approximately 0.7) [44], Figure 4.1 shows the excitation and emission spectra of SYBR Gold nucleic acid gel stain bound to double-stranded DNA, the excitation peak wavelength of SYBR Gold is around 495nm for single-photon excitation, the emission peak wavelength is round 537nm.

In our staining procedure of the CroV sample, we tried both DAPI and SYBR Gold stain. However DAPI is not sufficiently bright to be used for our purpose of studying the fast interaction between C. roenbergensis and CroV. The CroV sample stained by diluted SYBR Gold stain showed more brightness.

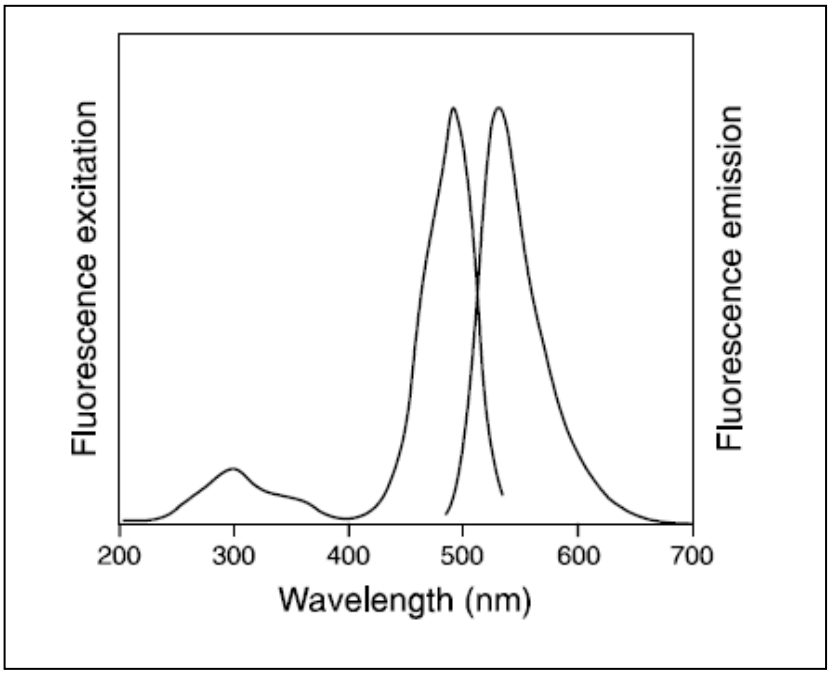

Figure 4.1 Spectra of SYBR Gold nucleic acid gel stain bounding with double-stranded DNA

Since SYBR Gold stain is expensive and sensitive to photobleaching and freeze-thaw cycle [45], we used two steps to dilute the manufacturer's stock to avoid this problem. First, we diluted manufacturer's stock of SYBR Gold Nucleic Acid Gel Stain (Life Technologies, catalog number S-11494) concentration 1:20 by pipetting out 1 µl from 20 µl of 0.02µm filter-autoclaved MilliQ H_2O, and substitute in 1 µl SYBR Gold Nucleic Acid Gel Stain manufacturer's stock, this stock can be stored at -20℃ for up to 1 week; We further diluted 1:20 to make a 1:400 dilution of the manufacturer's stock SYBR Gold stain reagent. We stained CroV sample by using the same volume of 1:400 dilution of SYBR Gold stain in a dark room, and wait for 15mins until CroV were stained completely. For imaging the interaction, in order to reduce SYBR gold dye's impact on C.roenbergensis, a dye remove procedure is used to remove SYBR gold dye in CroV culture before we mix C.roenbergensis and CroV. The dye in the CroV sample solution was removed by centrifugation at 18,000xg and pelleting twice.

Our images also showed that adding ethanol to the solution may increase the brightness of SYBR Gold. This is explained in the following section.

4.1.2 Removing Bacteria from the Sample

CroV culture which comes from the ocean water contains bacteria. Therefor a major struggle in finding the moment of interaction between C. roenbergensis and CroV is to have a pure sample of viruses. In order to not be deceived by interaction between bacteria and C. roenbergensis instead of interaction between CroV and C. roenbergensis, we have to purify the CroV culture and eliminate bacteria. We have tried different methods which are described in this section.

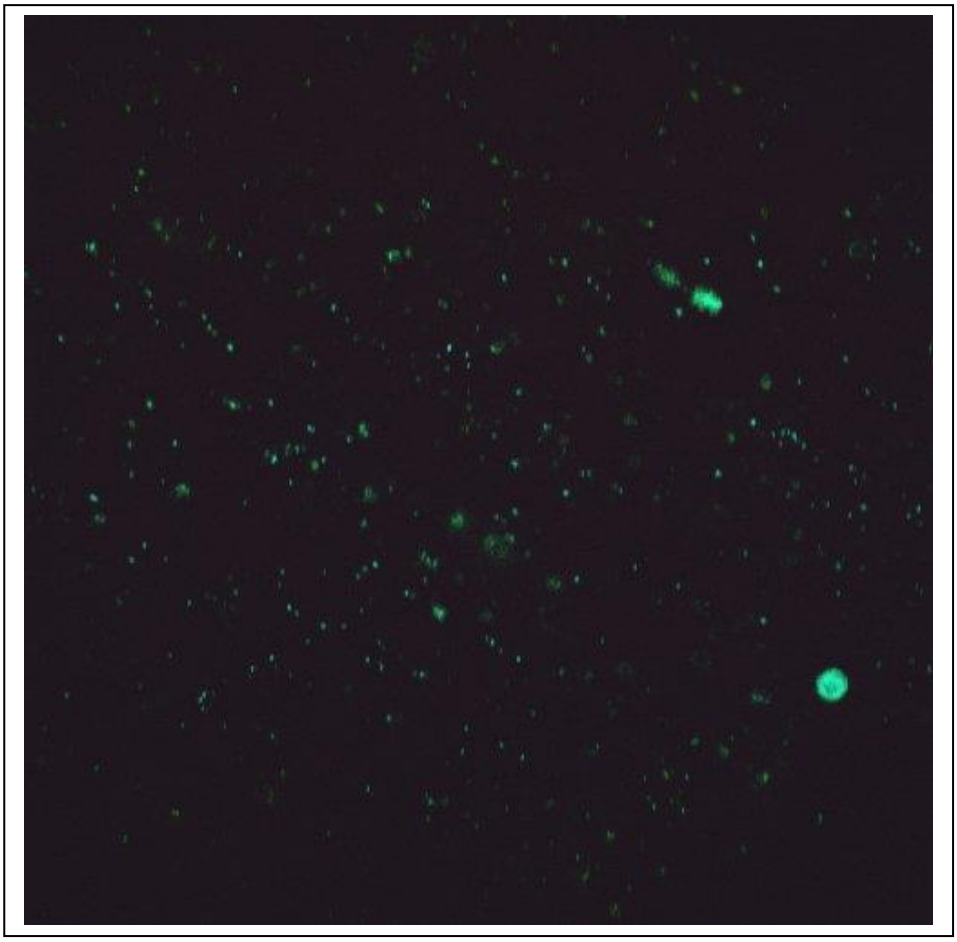

Figure 4.2 0.2 µm filter autofluorescence signal

Filtering Method

Imaging marine samples on the filter is a common method in virus enumeration [46]. However, we decided to use filters to reduce the number of bacteria in the sample. We used 0.8

μm filter to eliminate bacteria because of their size. Following the idea of enumerating viruses [46], we studied the filtered culture on the 0.2 μm filters. However, images taken from the filter itself showed a strong autofluorescence signal. This is shown in Figure 4.2. Therefore data acquired from the images of viruses and bacteria on the filters is not reliable due to this strong background noise.

We imaged the solution on slide glass instead of imaging it on the 0.2 filter. Figure 4.3 (a) shows images taken from the sample filtered 1 to 3 times with the 0.8 filter. All samples are centrifuged (5000×g, 15 min) to make a higher concentration. Images are shown in Fig 3.3 where (a), (b) and (c) correspond to 1× 0.8 um, 2× 0.8 um and 3× 0.8 um filtered solution respectively. All samples are stained by 1:400 diluted SYBR Gold nucleic acid stain.

Figure 4.3 CroV solution after (a) 1× filtering with .8 μm filter

(b)

(c)

Figure 4.3 CroV solution after (b) 2× (c) 3× filtering with .8 μm filter

Processing the images taken from filtered samples shows an increase in the ratio of the virus to bacteria in the solution. The approach and results are described in Image processing section.

Ethanol Treatment Method

(a)

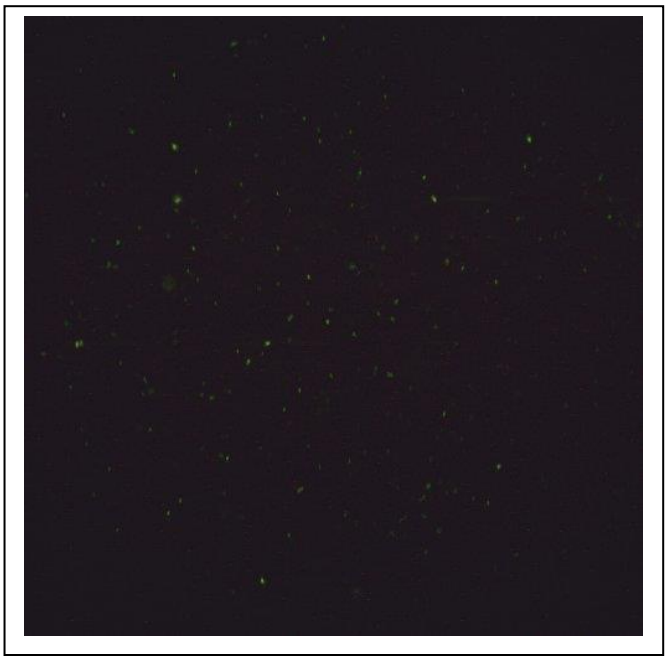

(b)

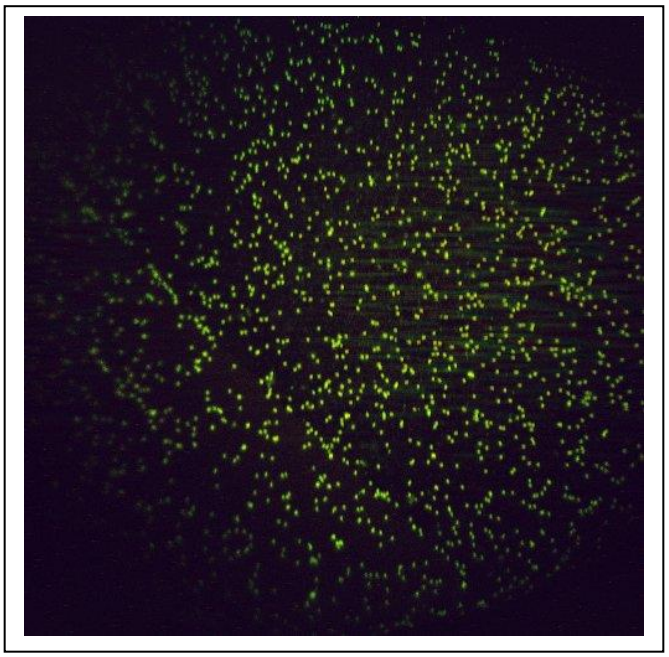

Figure 4.4 Comparison of (a) 0 % and (b) 40 % ethanol treated solution

Ethanol treatment is used as a method of killing bacteria [46]. We tried different percentage of ethanol in the solution to kill bacteria. However, taking image from the sample showed different results where it seems that ethanol has increased the effectiveness of the SYBR Gold. Figure 3.4 shows the same sample without alcohol treatment (a), and with 40 percent alcohol treatment (b). This enhancement in the fluorescent signal strength could be due to further penetration of SYBR Gold stain through the cell membrane. Further studies are required to investigate the procedure.

Differential Centrifuge Method

Differential centrifugation is a common procedure in microbiology and cytology used to separate certain organelles from whole cells for further analysis of specific parts of cells. Separation is based on size and density, with larger and denser particles pelleting at lower centrifugal forces. Here we use centrifuge to separate bacteria and virus, based on their difference in the size.

Differential centrifuge method was applied to the CroV culture which we used for imaging the interaction between CroV and C. roenbergensis. 1mL CroV sample (1x10^11 particle per mL) was further concentrated by centrifugation at 5,000xg for 30 min to remove majority of the bacteria. The supernatant was then centrifuged at 18,000xg for 2 hours and virus pellet was re-suspended in 20 μL.

4.2 TPFM IMAGING

4.2.1 C. Roenbergensis Imaging

We dripped 4uL C. roenbergensis sample on slide glass and covered it with cover glass. The images of C.roenbergensis are shown in Fig.4.5 (a) and Fig. 4.5 (b).

Figure 4.5 (a) is the image obtained in reflection channel, the laser wavelength is 710nm, the laser power is about 20mW on the sample, and the voltage of the photodiode is about 142V. Figure 4.5 (b) shows the NADH autofluorescence signal from C.roenbergensis in the blue detection channel, the excitation wavelength is 710nm, the laser power is about 20mW on the

sample and the voltage of the PMT A is 3.3V. From Fig. 4.5 (b), it can be seen clearly that the NADH signal from C. roenbergensis can be obtained by 710 nm two-photon excitation.

(a)

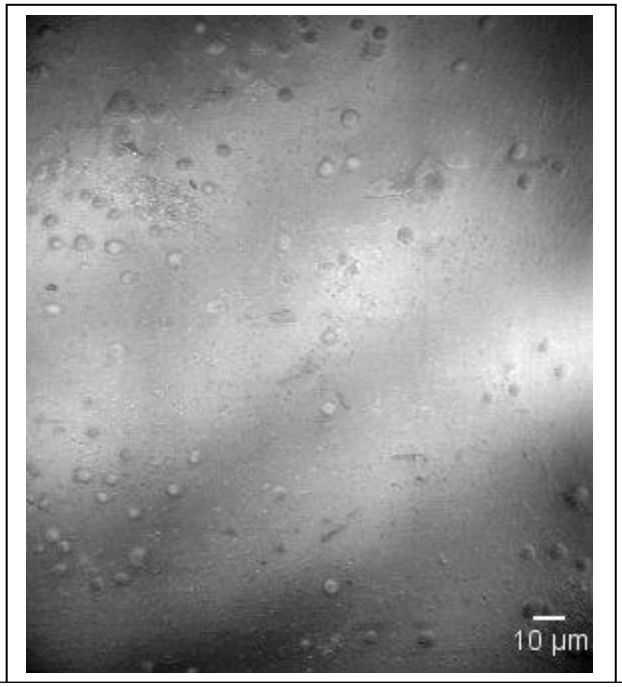

(b)

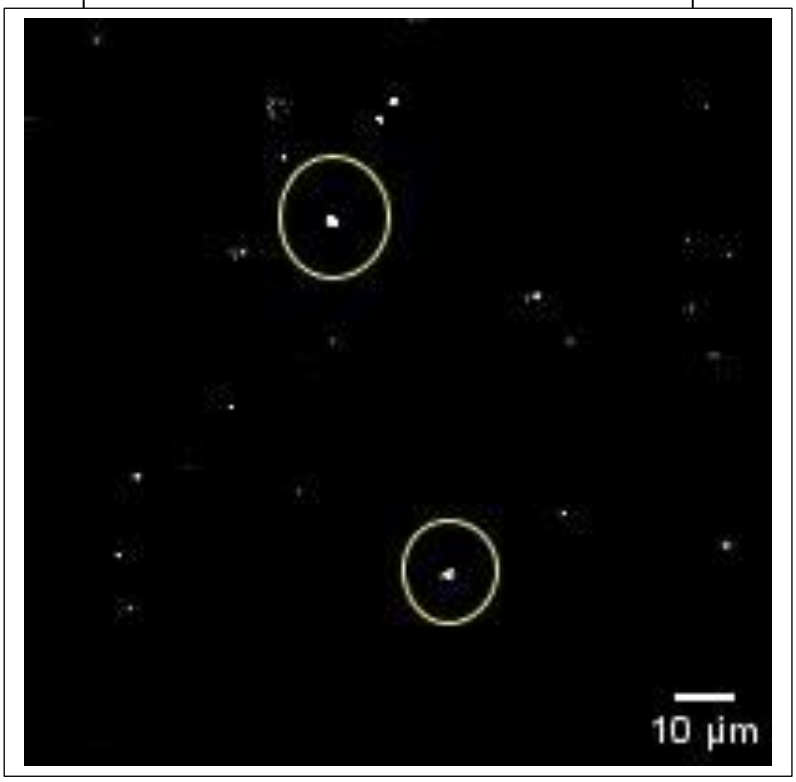

Figure 4.5 C. roenbergensis imaging in (a) reflection channel, and (b) NADH autofluorescence

The focal plane of the fluorescence channel in axial direction is about 1 μm, which is much thinner than that of the reflection channel, hence, although the sample contains many C.roenbergensis which are shown in Fig.4.5 (a), only a few of them can be viewed in blue detection channel in Fig4.5 (b).

4.2.2 CroV Imaging

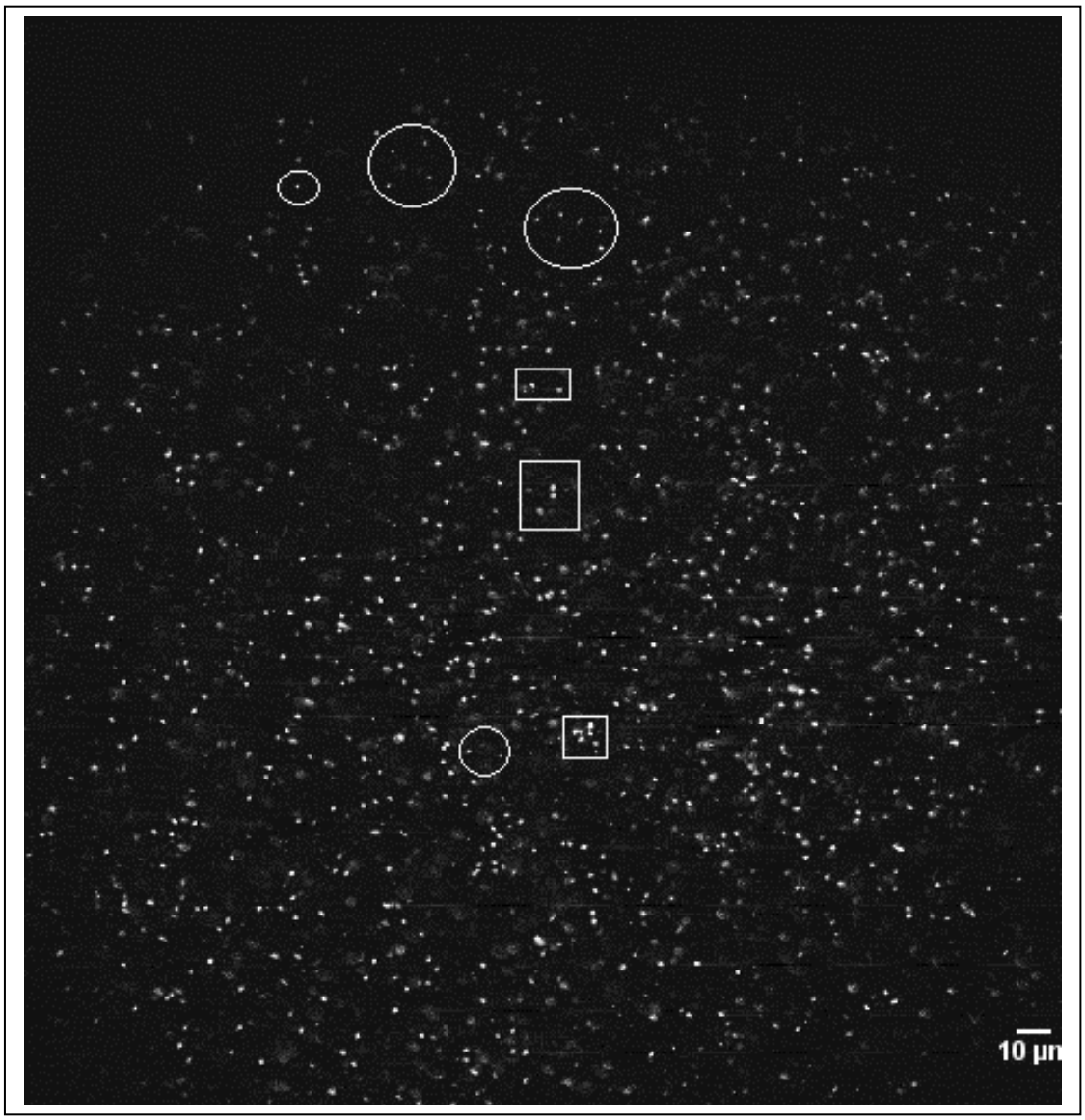

Figure 4.6. SYBR gold stains CroV imaging.

Circle indicates CroV and square indicates bacteria.

In CroV imaging, the slide glass and cover glass were cleaned by 90% Acetone to reduce potential environmental contamination. Fig. 4.6 shows the SYBR gold stained CroV image obtained from the green detection channel. In this image, the excitation laser wavelength is 710 nm, the power on the sample is about 20 mW, and the PMT A is about 1.84V. The size of CroV is about 280 nm [44]. The circle indicates CroV and the rectangle indicates bacteria in the sample.

4.2.3 Imaging the Interaction in Two Channels

We cleaned the slide glass and cover glass by using 90% Acetone to reduce potential environmental contamination, and dripped 4 μL C.roenbergensis and 2 μL CroV culture on the slide glass and covered it with cover glass. We put and recorded the sample under our two-photon fluorescence microscopy immediately after the sample is ready. The interaction process between C.roenbergensis and a marine object which is either CroV or bacteria is shown in Fig.4.7 (a) to (d). In Fig. 4.7 (a) to (d), the excitation laser wavelength is 710nm, the excitation power on the sample is about 20 mW, the voltage of PMT A and PMT B is 1.75V and 3.3V respectively.

Fig.4.7 (a) is one frame captured at time 0.57s. In Fig.4.7(a), a C.roenbergensis which is shown in the circle, is approaching to the marine object, which is shown in the ellipse; Fig. 3.7(b), which was captured at time 0.60s, shows the C.roenbergensis is contacting with the marine object; Fig 3.7(c) and (d), which were captured at time 1.17s and 1.43s respectively, show the marine object is traveling with C.roenbergensis.

To be sure that the moment of interaction we capture is the interaction between C. roenbergensis and CroV, we still need to purify the CroV sample as mentioned before. However this live video shows that our 30 frames per second imaging system is capable to catch the fast interaction of this marine virus-host system.

(a)

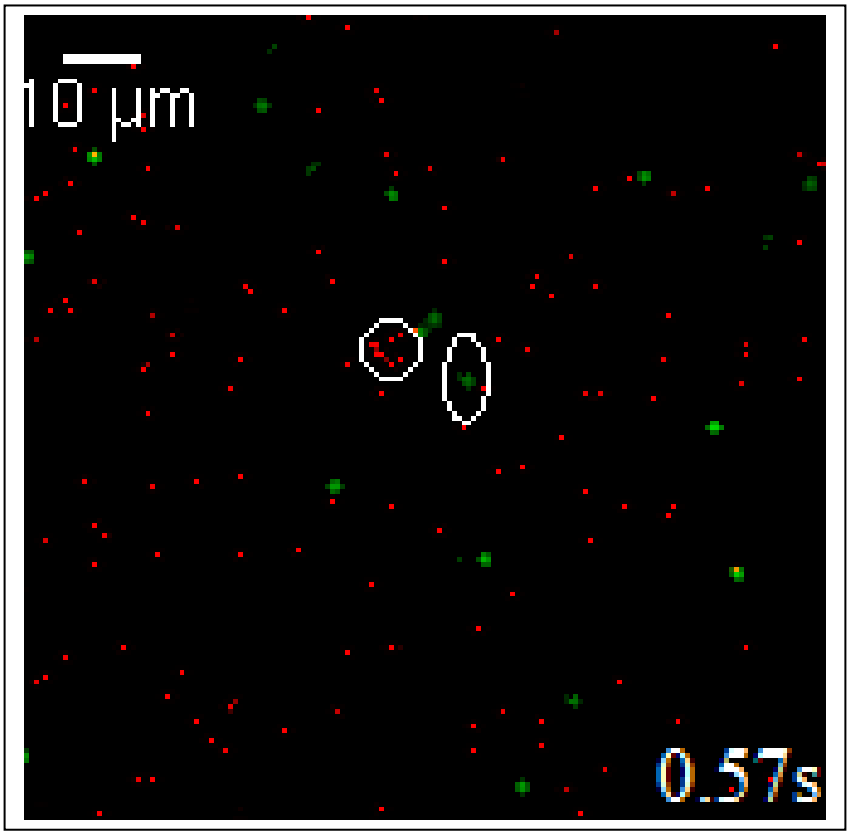

(b)

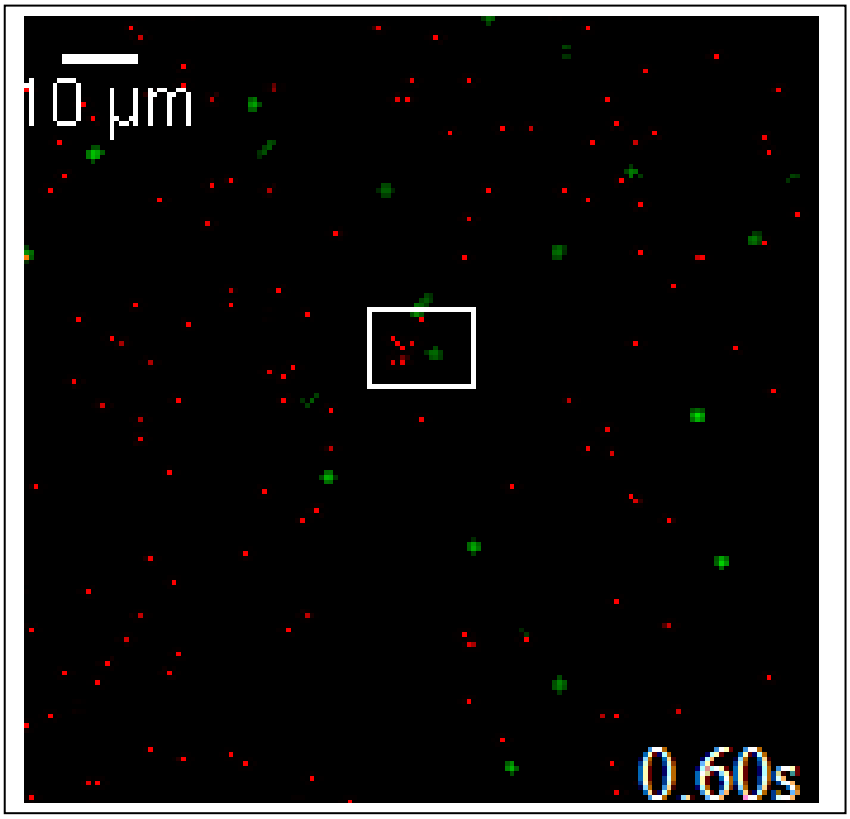

Figure 4.7 Imaging the interaction between C.roenbergensis and CroV. (a), (b)

(c)

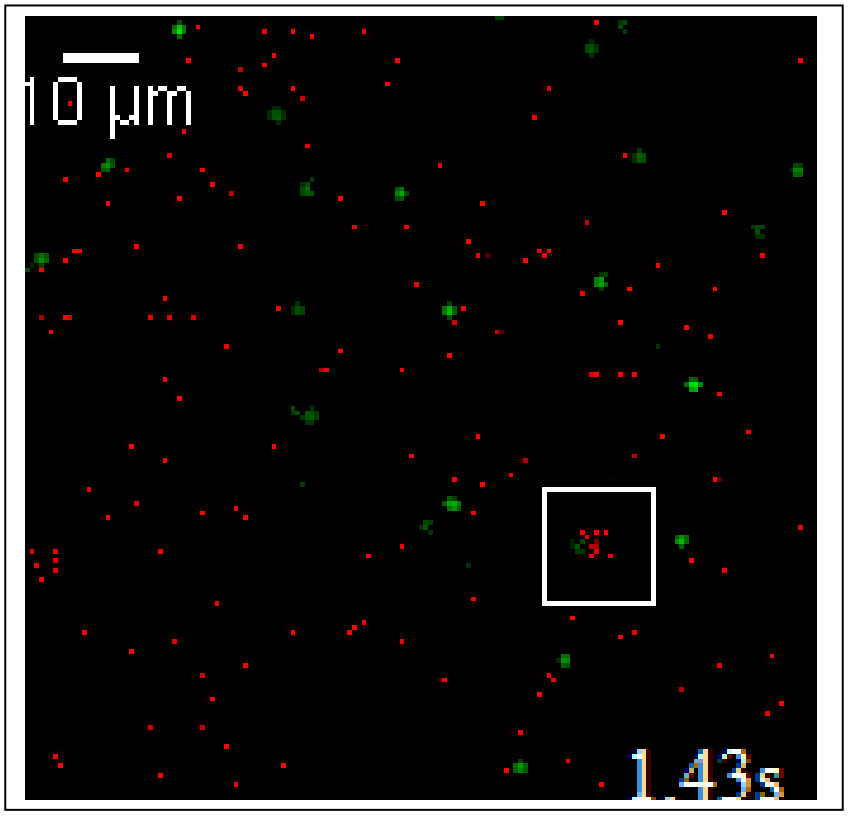

(d)

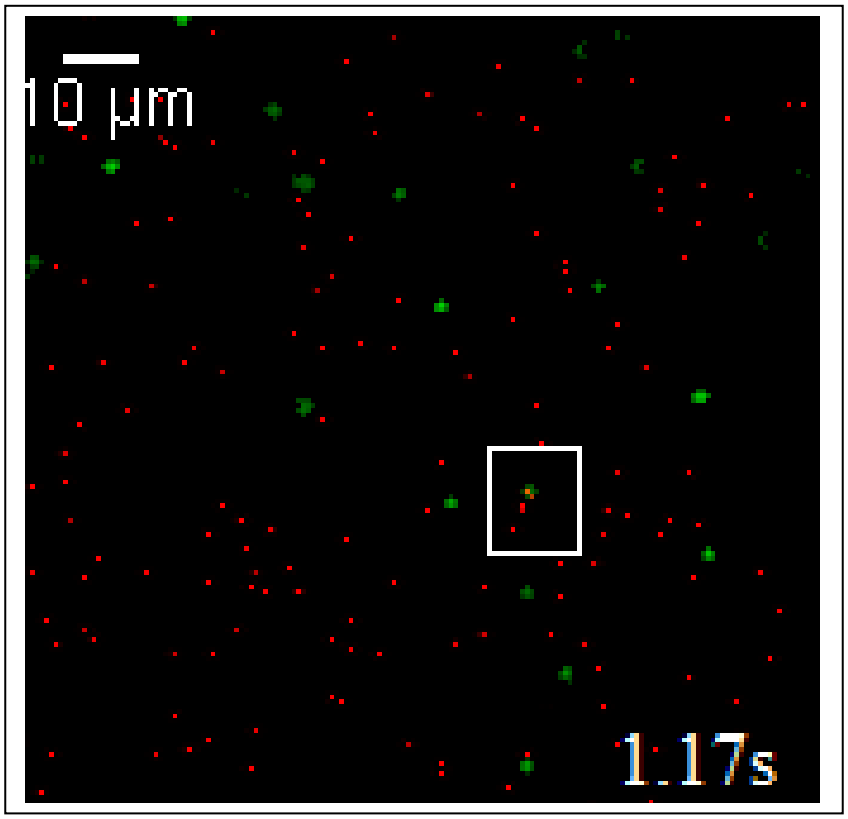

Figure 4.7 Imaging the interaction between C.roenbergensis and CroV. (c), (d)

4.3 IMAGE PROCESSING OF TPFM IMAGES

4.3.1 Noise Reduction

There is a background noise in our TPFM images and to catch the moment of interaction between C. roenbergensis and CroV, this noise should be minimized. However, because of the size of the virus (300 nm , less than 4 pixels in TPFM image), image processing with common noise reduction filters would eliminate some of the important data on the image. To overcome this struggle we combined 4 filters and developed a new method by making a mask from the same image for processing this image. Making a macro of these consecutive filters in ImageJ, we are able to process the video taken by our TPFM, frame by frame automatically. Figure 4.8 shows one frame of the movie of taken by our TPFM from swimming C. roenbergensis where (a) is the raw image and (b) is the post processed image using the following macro in ImageJ:

```
run("Despeckle", "stack");
run("Find Edges", "stack");
run("Gaussian Blur...", "sigma=1 stack");
setOption("BlackBackground", true);
run("Make Binary", "method=Yen background=Default calculate black");
imageCalculator("AND create stack", "Source.avi","Source-1.avi");
```

In this algorithm all the filters are applied on a temporary image which will be used as the mask for the main image. This is the key point in order to minimize the data loss during the image processing.

We have also developed the Matlab code for this procedure. Adding this code (in C++) to our TPFM, we will get real-time image processing.

(a)

(b)

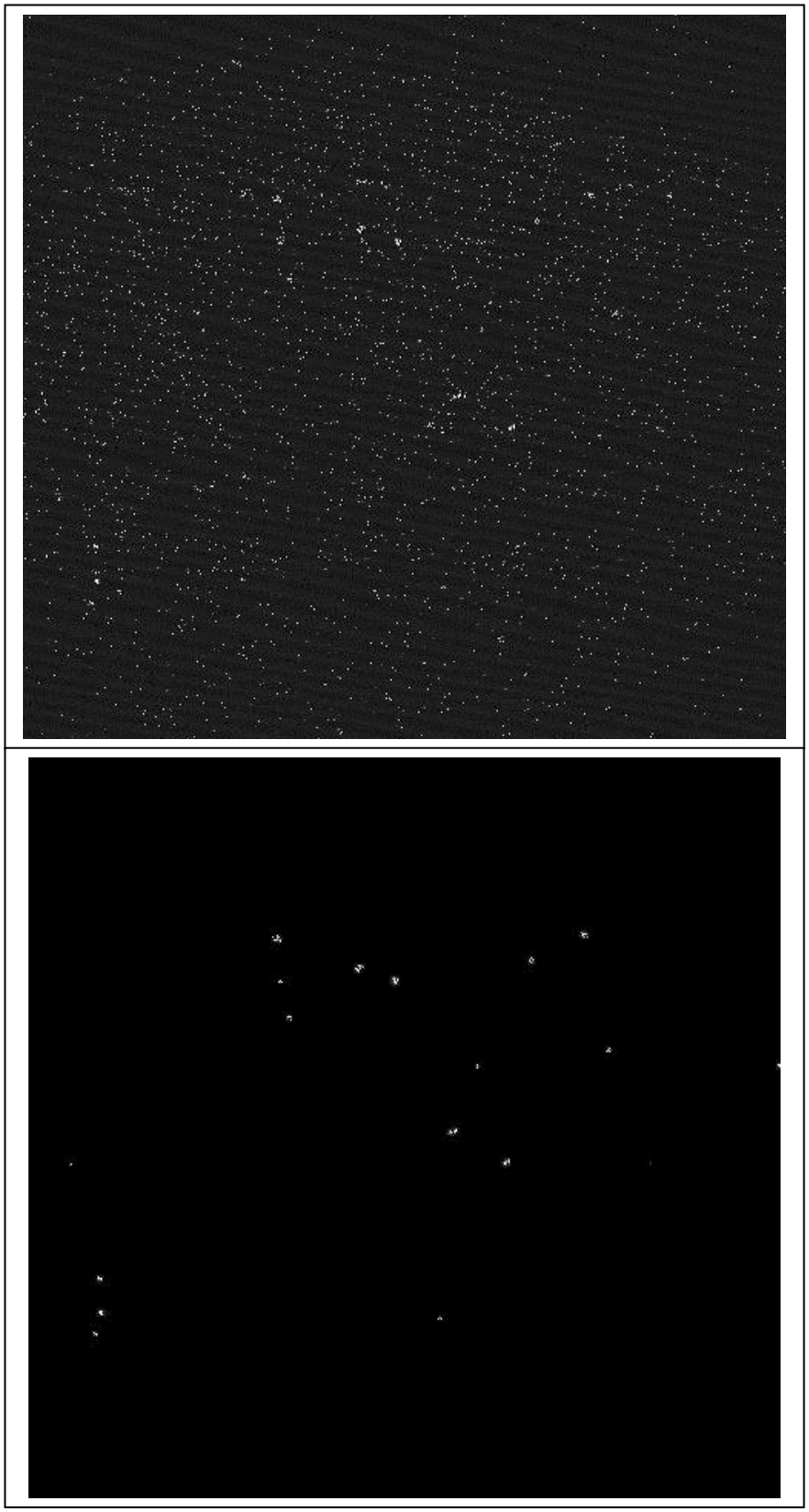

Figure 4.8 (a) Raw image and (b) post processed image of C. roenbergensis

4.3.2 Virus - Bacteria Enumeration

Image processing was also used in automatic virus-bacteria enumerating procedure. This method was used to get the virus-bacteria ratio in images of the CroV sample. The following ImageJ macro is made.

```
setAutoThreshold("Default dark");
//run("Threshold...");
setThreshold(40, 255);
setOption("BlackBackground", true);
run("Convert to Mask");
run("Close");
run("Make Binary");
run("Watershed");
run("Analyze Particles...", "size=0-Infinity circularity=0.00-1.00 show=[Bare Outlines] display");
```

Getting the result of this procedure, we are able to sketch a histogram of the image based on the size of the objects. Figure 4.9 (b) shows the histogram corresponding to Figure 4.9 (a) which is taken from CroV solution. It can be seen that the histogram has two maximum, where the smaller size corresponds to the virus and the bigger size corresponds to bacteria. We considered objects smaller than 4 pixels as virus, and those with the size bigger than or equal to 4 pixels as bacteria. Table 4.1 shows the result we got from analyzing images of filtering method of Fig. 4.3.

Table 4.1 Results of filtering method

CroV Sample	Number of Viruses	Number of Bacteria	V/B Ratio
1x fitering	57	58	0.98
2x filtering	24	10	2.4
3x filtering	10	15	0.66

(a)

(b)

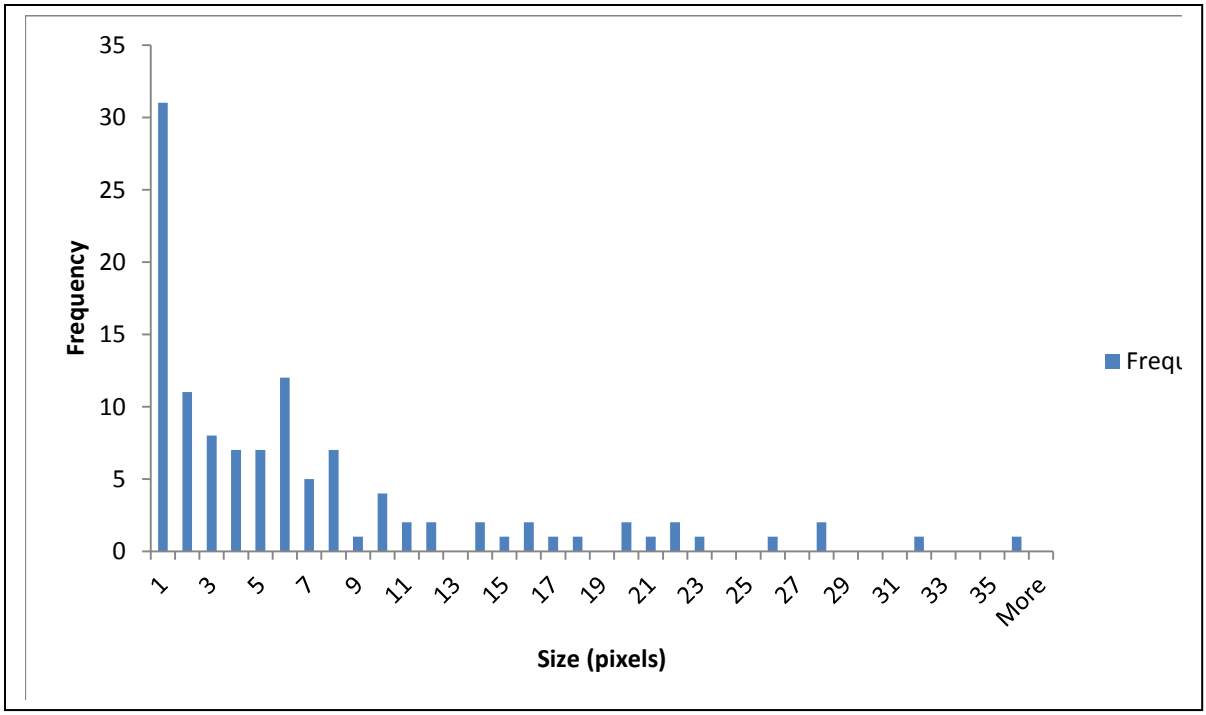

Figure 4.9 (a) TPFM image of CroV solution and (b) histogram based on the size of objects

According to Table 4.1, 2× filtering thr Cro-V solution will have the best result in increasing the ratio of viruses to the bacteria. 3× filtering seems to decrese the ratio. It seems that after 3× filtering the number of viruses have decreased so much that the solution might not be infectious enough.

4.4 CRYO-EM IMAGING

Once we get the moment of interaction, we will fix the sample to investigate it to nanometer resolution under the transmission electron microscope at the Department of Chemistry of UTEP. The JEM-3200FS is a 300 keV cryo-TEM with an omega energy filter for increased contrast and high resolution, which was installed in 2011. Our TEM is designed for use with biological samples and is capable of resolving to better than 1nm.

Cryo-EM imaging is done in collaboration with Dr. Chuan Xiao's lab where they are also doing structural studies of the giant marine virus CroV. Cryo-EM images of C. roenbergensis and CroV taken with UTEP TEM are shown in Figure 4.10 and Figure 4.11 respectively.

(a)

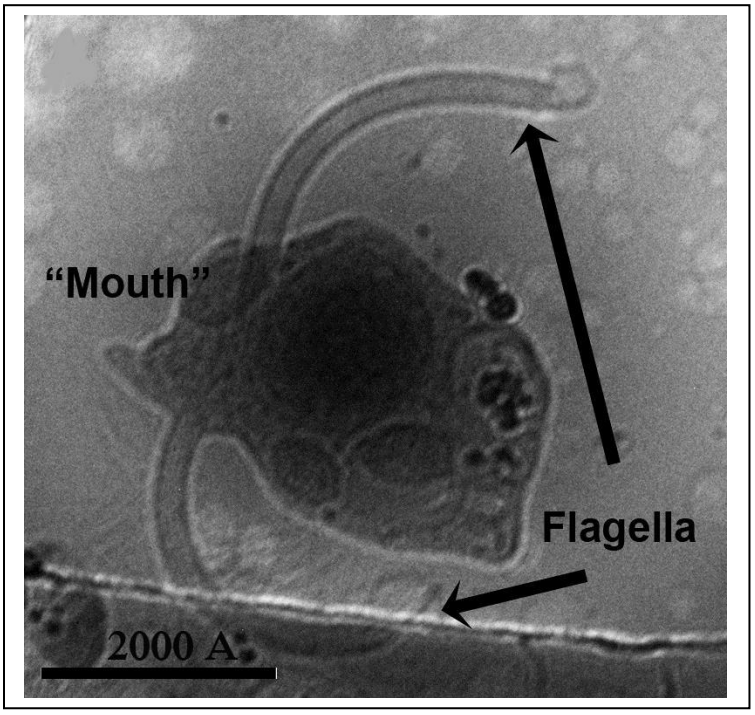

Figure 4.10 Cryo- EM image of C. roenbergensis

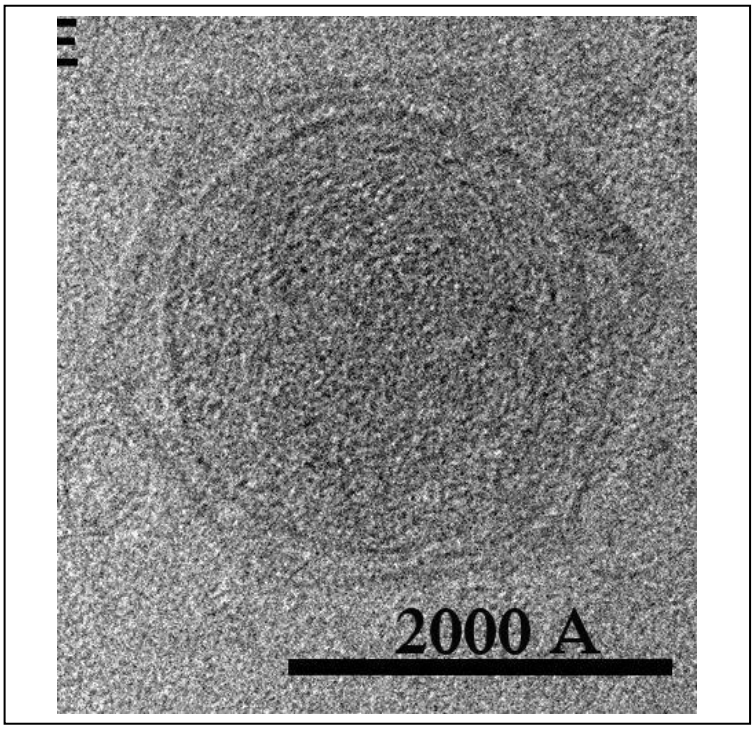

Figure 4.11 Cryo- EM image of CroV

4.5 CONCLUSION

In this study, cafeteria roenbergensis and cafeteria roenbergensis virus are visualized by using two-photon fluorescence microscopy, the C.roenbergensis was imaged by exciting and detecting the NADH autofluorescence signal; and the CroV was viewed by staining with SYBR Gold nucleic acid gel stain. Both C.roenbergensis and CroV can be imaged by using 710nm excitation wavelength.

By using two-photon fluorescence microscopy, we have demonstrated the initial interaction between C.roenbergensis and a marine object (bacteria or CroV). In order to get the interaction between CroV and C. roenbergensis we have to purify the virus sample. However this video rate imaging shows the capability of our TPFM imaging to capture this fast interaction. Moreover this method seems to be potentially useful technique to track the viral replica process longitudinally in the living host and even in humans.

We have tried different methods to purify the virus sample. In the procedure of filtering the sample we criticized the common method of virus enumeration on the filter, where we imaged a descent autofluorescence signal from the raw filter. Filtering method can be utilized

twice to increase the ratio of the virus to bacteria. Ethanol treatment was another approach which we used to eliminate bacteria from the solution where it showed to enhance the fluorescence signal strength. Ethanol treatment seems to enhance the effectiveness of the SYBR Gold nucleic acid stain.

To get a clear view of the small objects in our two photon excitation microscopy images, we developed a new algorithm to reduce the noise in the images which minimizes the data loss. This method is useful when the size of the objects is in the same order of background noise. This capability can be added to our microscope to get a real time image processing.

By combining TPFM with transmission electron microscopy, which could resolve the virus-host interaction at molecular level, the complete process of host-viral interaction system can be demonstrated, which will significantly expand the applications of two-photon fluorescence in immunology research and lead to important medical applications.

References

[1] Danovaro, R., et al, "Marine viruses and global climate change," FEMS microbiology reviews, 35(6), 993-1034 (2011).

[2] Wilhelm, S. W. and Suttle, C. A.,"Viruses and nutrient cycles in the sea," Bioscience, 49(10), 781-788 (1999).

[3] Suttle, C. A.,"Viruses in the sea," Nature, 437(7057), 356-361 (2005).

[4] Wilhelm, S. W., et al "Measurements of DNA damage and photoreactivation imply that most viruses in marine surface waters are infective," Aquatic microbial ecology, 14(3), 215-222 (1998).

[5] O'Kelly, C. J. & G. Burger "Cafeteria roenbergensis MtDNA," Evolutionary & Integrative Genomics. (1994).

[6] Fenchel, T. "Marine plankton food chains," Annual Review of Ecology and Systematics 19: 19–38 (1988).

[7] Otto, K., D. Weichart & S. Kjelleberg "Plasmid transfer between marine Vibrio strains during predation by the heterotrophic microflagellateCafeteria reonbergensis,". Applied and Environmental Microbiology 63 (2): 749–752. (1997).

[8] Massana, Ramon, et al "Crash of a population of the marine heterotrophic flagellateCafeteria roenbergensis by viral infection, " Environmental Microbiology 9 (11): 2660–2669 (2007).

[9] Guiry, M. D. & Guiry, G. M. "AlgaeBase," National University of Ireland, Galway. (2012).

[10] Cavalier-Smith, et al." Algaebase :: Listing the World's Algae. " Algae Base. Web (2012.)

[11] Park, J. S. & Simpson, A. G. B. "Characterization of halotolerant Bicosoecida and Placididea (Stramenopila) that are distinct from marine forms, and the phylogenetic pattern of salinity preference in heterotrophic stramenopiles," Environmental Microbiology 12: 1173–1184, (2010)

[12] Fischer, M. G.; et al "Giant virus with a remarkable complement of genes infects marine zooplankton," Proceedings of the National Academy of Sciences 107 (45): 19508–19513, (2010)

[13] Fischer, M. G, "Suttle Laboratory Marine Virology and Microbiology: Profile: Matthias Fischer". Suttle Laboratory. Retrieved (2010)

[14] Timmer, J. "A virus so large it gets viruses". Ars Technica. Retrieved (2010)

[15] Massana, R., Javier D. C., Christian D. and Ruben S., "Crash of a population of the marine heterotrophic flagellate Cafeteria roenbergensis by viral infection." Environmental microbiology, 9(11), 2660-2669 (2007).

[16] Hoover, E. E. and Jeff A. S., "Advances in multiphoton microscopy technology." Nature Photonics 7(2): 93-101 (2013).

[17] Li, C. et al. "Multiphoton microscopy of live tissues with ultraviolet autofluorescence." IEEE J Sel Top Quantum Electr 16(3): 516-523 (2010).

[18] Zipfel, W. R., Williams, R. M. and Webb, W. W., "Nonlinear magic: multiphoton microscopy in the biosciences," Nature biotechnology, 21(11), 1369-1377 (2003).

[19] James, E.N. et al. "Resolution in Optical Microscopy," Methods in Enzymology, 360(Biophotonics Part A), 416-446 (2003).

[20] Veilleux, I., et al. "In vivo cell tracking with video rate multimodality laser scanning microscopy," IEEE Journal of selected topics in quantum electronics, 14(1), 10-18 (2008).

[21] Adrian, M, et al, (1984). "Cryo-electron microscopy of viruses," Nature 308 (5954): 32–36

[22] Goeppert-Mayer M. "Über Elementarakte mit zwei Quantensprüngen".Annals of Physics 9 (3): 273–295 (1931).

[23] Hellwarth R and Christensen P. Nonlinear optical microscope examination of structures in polycrystalline ZnSe. Opt Commun 12: 318–322, (1974)

[24] Denk W, Strickler J, and Webb W. "Two-photon laser scanning fluorescence microscopy." Science 248: 73–76, (1990)

[25] Grace E. Stutzmann and Ian Parker, Physiology 20:15-21, (2005)

[26] Nicole Rusk, "The fluorescence microscope," Nature Methods: Milestones Light Microscopy, 58-59(2009)

[27] Webb R. "Theoretical basis of confocal microscopy," Methods Enzymol 307: 3–20, (1999)

[28] Stutzmann, G. E. & Parker, I. " Dynamic Multiphoton Imaging :A Live View from Cells to Systems,"Int.Union.Physiol.Sci./Am.Physiol.Soc , 1548-9213/05 (2005),

[29] Diaspro, A. et al "Two-Photon Excitation Fluorescence Microscopy" in Hawkes, P. W. & Spence J. C. "Science of Microscopy," Vol 2, New York: Springer (2007)

[30] Nakamura, O. "Two-Photon Excitation Microscopy," Microscopy Research and Technique Special Issue, Volume 47, Issue 3, pages 165–171, (1999)

[31] Diaspro, A. "Confocal and Two-Photon Microscopy: Foundations, Applications and Advances", New York: Wiley (2001)

[32] Born, M. & Wolf, E. "Principles of Optics: Electromagnetic Theory of Propagation, Interference and Diffraction of Light", Cambridge: University Press (1980)

[33] Diaspro, A. et al. “Two-photon fluorescence exitation and related thechniques in biological microscopy,” Q. Rev. Biophys.15, 1–70 (2006).

[34] C. J. R. Sheppard, M. Gu "Image formation in two-photon fluorescence microscopy," Optik - International Journal for Light and Electron Optics 86(3):104-106 (1990)

[35] Denk W, Strickler J, and Webb W. "Two-photon laser scanning fluorescence microscopy," Science 248: 73–76, (1990)

[36] Xu C, Zipfel W, Shear JB, Williams RM, and Webb W. "Multiphoton fluorescence excitation: new spectral windows for biological nonlinear microscopy," Proc Natl Acad Sci USA 93: 10763–10768, (1996)

[37] Adrian M., et al "Cryo-electron microscopy of viruses," Nature 308, 32 - 36 (1984)

[38] Kirkland, A. I. & Hutchison J. L. "Atomic Resolution Transmission Electron Microscopy, " in Hawkes, P. W. & Spence J. C. "Science of Microscopy," Vol 1, New York: Springer (2007)

[39] Karnovsky M J. "A formaldehyde-glutaraldehyde fixative of high osmolality for use in electron microscopy, " J. CellBiol. 27:137-8A, (1965)

[40] Bozzola, John J. & Russell, Lonnie D. "Specimen Preparation for Transmission Electron Microscopy," Electron microscopy : principles and techniques for biologists. Sudbury, Mass.: Jones and Bartlett. pp. 21–31. (1999)

[41] Noble, Rachel T. & Jed A. Fuhrman., "Use of SYBR Green I for rapid epifluorescence counts of marine viruses and bacteria." Aquatic Microbial Ecology 14(2): 113-118 (1998).

[42] SUTTLE, A. et al. "Infection of phytoplankton by viruses and reduction of primary productivity" Nature 347, 467 - 469 (1990)

[43] Shibata, A.1, et al. "Comparison of SYBR Green I and SYBR Gold stains for enumerating bacteria and viruses by epifluorescence microscopy, " Aquat Microb Ecol, Vol. 43: 223–231, (2006)

[44] Tuma, R. S., et al. "Characterization of SYBR Gold nucleic acid gel stain: a dye optimized for use with 300-nm ultraviolet transilluminators," Analytical biochemistry, 268(2), 278-288 (1999).

[45] Anand, P. et al. "Virus and prokaryote enumeration from planktonic aquatic environments by epifluorescence microscopy with SYBR Green I," Nature protocols 2(2): 269-276 (2007).

[46] Slimani M. et al. " Alcohol Disinfection Procedure for Isolating Giant Viruses from Contaminated Samples," Intervirology 56:434-440 (2013)

Vita

S.Ali Aghvami was born in Tehran, Iran. He was nominated for National Science Student Award because of his physics student project while he was a high school student at NODET (National Organization for Development of Exceptional Talents) high school, Tehran. He was selected as “Elite Student” at Tehran Azad University because of design and make of a 6” Newtonian telescope and its polar mount. In the spring of 2013, he joined the University of Texas at El Paso to pursue a Master of Science degree in physics. He has been awarded “Dodson Research Grant” from UTEP Graduate School and “C. Sharp Cook Fellowship” and “Graduate Research Excellence Award” from Department of Physics.